Available online at www.sciencedirect.com
ScienceDirect
Journal of Nuclear Materials 356 (2006) 136–147
journal of nuclear materials
www.elsevier.com/locate/jnucmat

Displacement and helium-induced enhancement of hydrogen and deuterium retention in ion-irradiated 18Cr10NiTi stainless steel

G.D. Tolstolutskaya [a], V.V. Ruzhytskiy [a], I.E. Kopanets [a], S.A. Karpov [a], V.V. Bryk [a], V.N. Voyevodin [a], F.A. Garner [b,*]

[a] *NSC 'Kharkov Institute of Physics and Technology', Kharkov, Ukraine*
[b] *Pacific Northwest National Laboratory, Box 99, Richland, WA 99354, USA*

Abstract

There is strong interest in the accelerator-driven transmutation technology community on the synergistic effects of displacement damage and co-generated helium and hydrogen on property changes such as void swelling, irradiation creep, hardening, and possibly on corrosion and cracking. Substituting deuterium for protium offers advantages in experimental studies of the helium–hydrogen-damage synergisms. The influence of preimplanted helium and self-ion induced damage on deuterium trapping in 18Cr10NiTi stainless steel was studied using thermal desorption spectrometry, the nuclear reactions $^3He(D,p)^4He$ and $D(^3He,p)^4He$, and transmission electron microcopy. Reemission, retention and evolution of depth distribution profiles of deuterium in 18Cr10NiTi SS were studied for 10 keV D_2^+ and 10 keV He^+ implantation at room temperature followed by annealing at 300–1500 K. The amounts of trapped and released deuterium and helium atoms were measured as a function of implantation dose at various temperatures. It was found that retention of hydrogen and deuterium is strongly enhanced by the presence of large amounts of helium and also strongly enhanced by damage introduced by 2 MeV Cr^{3+} ions. These results are consistent with recent observations of hydrogen storage in stainless steels after irradiation in LANSCE with high energy protons and neutrons and also after irradiation in light water reactors.
Published by Elsevier B.V.

1. Introduction

Hydrogen and helium atoms are generated by nuclear transmutation in fusion and fission reactors, spallation neutron sources and high energy charged particle environments. Hydrogen is also generated by environmental sources such as corrosion, radiolytic decomposition and recoil injection, especially in systems involving water cooling and moderation, such as in pressurized water reactors (PWRs) and boiling water reactors (BWRs). In Western-design PWRs and in some BWRs a hydrogen overpressure is also maintained on the coolant to suppress the buildup of corrosive chemical species. Both helium

* Corresponding author. Present address: Pacific Northwest National Laboratory, Materials Resources, 902 Battelle Boulevard, MSIN: P8-15, 99354 Richland, WA, USA. Tel.: +1 509 376 4136; fax: +1 509 376 0418.
E-mail address: frank.garner@pnl.gov (F.A. Garner).

0022-3115/$ - see front matter Published by Elsevier B.V.
doi:10.1016/j.jnucmat.2006.05.022

and hydrogen are known to play an important role in the evolution of damage microstructure and may affect the mechanical properties and cracking behavior of structural materials. Hydrogen–helium interactions are interesting problems not only from the engineering viewpoint, but also from the fundamental viewpoint. Such interactions are particularly important in accelerator-driven systems (ADS) when the levels of co-generated helium and hydrogen can be very large and is usually rather variable from one ADS device to another, or strongly variable with position in a given device.

In a recent study by Garner, Oliver and their coworkers a range of pure metals, iron-base and nickel-base structural alloys were irradiated in a mixed spallation neutron and high energy proton beam at LANSCE for temperatures below 100 °C. The helium/dpa ratios obtained in structural alloys were as large as ~160 appm/dpa and were found to be essentially independent of alloy composition [1,2]. Such levels are an order of magnitude greater than those of either fusion spectra or PWR–BWR moderated fission spectra. In all of these environments, however, hydrogen is generated at roughly an order of magnitude higher rate than helium.

While it was expected that essentially all of the helium would be retained, it was found by Garner that an unexpectedly large retention of hydrogen was also occurring in structural alloys, but in a manner suggestive of microstructural trapping, varying with each alloy. The nature of such trapping could not be fully determined, nor was it possible in that study to separate the separate and potentially synergistic effects on retention of the two co-generated gases. The only clear conclusion was that no resolvable bubbles or cavities were forming in any of the studied alloys over the ranges of doses and relatively low temperatures studied. If helium clusters were interacting with hydrogen atoms, the clusters were sub-resolvable.

Unlike helium in nuclear reactor applications, the problem of hydrogen has not been as widely studied because it was considered that hydrogen produced by either nuclear reactions and environmental sources had a rather high diffusivity in stainless steels, and in the 300–600 K range should easily migrate without accumulating to high concentrations [3]. It is now known that there are conditions where this assumption is incorrect.

Garner and coworkers have recently shown that in fission reactors rather high concentrations of hydrogen can accumulate in stainless steels, especially when helium is co-generated at high levels or when voids and bubbles are available to store hydrogen [4,5]. In one case it was measured that ~3800 appm hydrogen had been stored in stainless steel after irradiation in a water-moderated reactor at 33 dpa, producing large levels of helium and a very high density of cavities. The interaction of these two gases was proposed by Garner to possibly accelerate the onset of void swelling of austenitic internals of pressurized water reactors [6,7]. Voids and bubbles alone are insufficient to retain hydrogen in fast reactor irradiation, however, since the sodium coolant has a strong affinity for hydrogen, which is continually being removed from the sodium by cold-trapping [4,5].

The retention and accumulation of hydrogen in irradiated stainless steels is most likely caused by the presence of high concentrations of microstructural trapping sites. Radiation-induced Frank loops and line dislocation microstructure may be traps for retention of moderate amounts of hydrogen (~1000 appm or less), most likely with hydrogen in atomic form. Formation of cavities, however, could strongly increase the trapping, especially if hydrogen is stored in the molecular state. Helium production via nuclear transmutation has also been proposed by Neklyudov and co-workers to contribute to hydrogen retention in structural materials [8]. In contrast to hydrogen, helium is essentially immobile at temperatures below $0.4T_m$ and participates strongly in cavity nucleation and stabilization. Hydrogen has been shown to increase the pressure in such cavities and shift the annealing temperature of the radiation-produced microstructure to higher temperatures [9].

Most previous investigations of the interactive influence of helium and hydrogen on radiation damage were carried out using ion implantation. Substantial attention was previously given to the problem of hydrogen and helium in fusion reactors and therefore most simulation experiments were carried out for irradiation up to doses of 10^{17}–10^{18} cm^{-2} which corresponds to gas concentrations of 10^4–10^5 appm. In a comparable time period at the same displacement rate the helium generation by transmutation in the PWR core baffle of steel 18Cr10NiTi will make only 30 appm/year (~15 appm/dpa reaching ~2000 appm during 60 year operation period) and of hydrogen at 74 appm/dpa (~4000 appm in 60 years) [10]. Unlike the ADS and fusion environments the generation rates of both helium and hydrogen in fission neutron spectra are very sensitive

to alloy composition with the largest portions of these gases being disproportionately produced by the nickel, especially in water-moderated spectra [11–13]. Given the large range of gas generation rates of various nuclear devices it was decided that helium–hydrogen interactions should be studied proceeding from relatively low levels to rather high levels in order to discern the onset and nature of the potential interactions.

In the current study we investigate the accumulation, migration, distribution and desorption of helium and hydrogen (deuterium) implanted in 18Cr10NiTi steel over a wide range of implanted gas concentrations at levels characteristic of some ADS devices, fusion reactors, PWRs and Russian-design VVER-1000 reactors. Note that VVER is the Russian acronym for water-cooled, water-moderated energy reactor.

Data were obtained on microstructural evolution and its effect on trapping and retention of helium and hydrogen (deuterium) in the temperature range 300–900 K and following post-implantation annealing at 300–1500 K. The substitution of deuterium for protium allows the use of nuclear reactions to determine the depth distribution and concentration of hydrogen isotopes.

2. Experimental procedure

The 18Cr10NiTi steel is used in states of the Former Soviet Union for nuclear applications where AISI 304 would be used in Western countries. Its composition is similar to AISI 321 at Fe–18.5Cr–9.5Ni–1.5Mn–0.7Si–0.6Ti with $\leqslant$0.12 C. Specimens of size $27 \times 7 \times 0.1$ mm were cut from 18Cr10NiTi steel following prior annealing for 1 h at 1340 K in 10^{-4} Pa vacuum. These specimens were polished in electrolyte having composition: 54% H_3PO_4, 11% H_2SO_4, 21% H_2O, and 14% CrO_3. Before irradiation the specimens were short-term annealed to 1200–1400 K in the experimental chamber.

Irradiation of 18Cr10NiTi steel with deuterium and helium was carried out using the assembly designated as 'IMPLANTATOR', having an oil-free evacuation system with residual pressure in the target chamber of $2–3 \times 10^{-4}$ Pa. Specimens were irradiated with 10 keV D_2^+ ions (5 keV/D^+) to $0.5–4 \times 10^{16}$ D/cm^2 and with 10 keV He^+ ions to doses of $1–50 \times 10^{15}$ cm^{-2}. The helium ion flux was 10^{13} cm^{-2} s^{-1} and deuterium ion flux was 10^{14} cm^{-2} s^{-1}. The implantation temperature was 300 K and was monitored using a chromel–alumel thermocouple. Post-implantation annealing of specimens was performed in the temperature range 300–1200 K by resistance heating with a rate of 7 K s^{-1}.

The implanted particle depth distribution was measured using the nuclear reactions ^{3}He (D, p)^{4}He and D (^{3}He, p)^{4}He with analyzing beams of D_2 ($E = 1$ MeV) and ^{3}He ($E = 700$ keV), respectively [14]. These measurements were performed on the electrostatic accelerator designated 'ESU-2 MeV' using forward scattering geometry. A beam of either ^{3}He or D_2 ions was incident at an angle of 30° to the specimen surface and the nuclear reaction products were recorded at an angle of 60° with respect to the analyzing beam. The beam diameter during irradiation was 3 mm and during analysis was 2 mm. The depth resolution in forward scattering geometry was determined to be ~15 nm.

To attenuate the back-scattered particle effect a nickel film of 0.5 μm thickness was placed in front of the surface-barrier detector. This leads to energy spectrum broadening of the reaction products. Line broadening from α-sources (^{238}Pu, ^{239}Pu, ^{233}U) for such a film was established earlier to be 32 keV. Therefore, under the experimental conditions employed the depth resolution was in the range 15–68 nm. All measurements of nuclear reaction energy spectra were performed using an equal quantity of analyzing ^{3}He or D_2 ions, constituting $\sim 10^{-4}$ C (with a spectra set up time of $\Delta t \sim$ 15–50 min).

Determination of concentration and depth distribution was performed using the procedure defined in Ref. [15]. The depth distribution was calculated from the energy spectra of α-particles. The concentration was determined using the method of 'internal calibration' employing the back-scattering spectra of analyzing beam ions scattered by the matrix atoms of the target. Calibration and determination of the absolute values of helium and deuterium concentration with back-scattering spectra was performed without the protective film on the detector.

Study of deuterium release from stainless steel was performed using a programmed thermal desorption technique on the assembly designated 'ANT' [16] in the temperature range 300–1500 K at a linear heating rate of 6 K s^{-1}. The residual gas pressure in the experimental chamber was $\sim 5 \times 10^{-5}$ Pa. Heating of specimens to measure hydrogen release was stopped at 1200 K because of hydrogen release from chamber components.

The microstructure of the implanted 18Cr10NiTi steel was observed using transmission electron

microscopy at room temperature, employing standard bright-field techniques on a JEM-100CX electron microscope.

3. Results

3.1. Helium only

Fig. 1 shows the typical energy spectrum of α-particles from the ^3He (D, p)^4He reaction and the corresponding depth profiles for 18Cr10NiTi steel specimens irradiated by 10 keV helium ions to doses of 1 and 4×10^{15} cm^{-2} at room temperature. The concentration of implanted helium increases proportionally with dose as shown in Fig. 1. The most probable range and the corresponding full width at half maximum (FWHM) allowing for finite depth resolution (horizontal bars at 2430 and 2540 channels) exhibit good agreement with those obtained from the TRIM Monte-Carlo code [17]. An additional peak at the 2580 channel is caused by α-particles that have passed through a discontinuity in the protective film without attenuation.

Depth profiles in 18Cr10NiTi steel are shown in Fig. 2 of ion-implanted helium with energy 10 keV to 1×10^{15} cm^{-2} at room temperature and after annealing temperatures 900 and 1100 K. Specimens were exposed 0.5 h at each annealing temperature. It is seen from Fig. 2 that the helium distribution profile produced upon annealing at 900 K is essentially identical to that produced at room temperature.

A variation in helium distribution profile was observed only at an annealing temperature of ~1100 K, resulting in a helium concentration

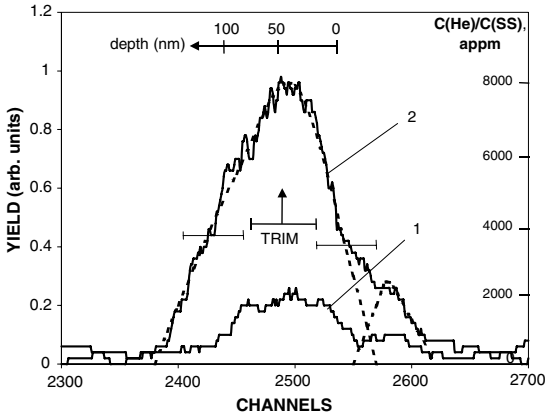

Fig. 1. Helium distribution profiles in 18Cr10NiTi steel irradiated with 10 keV helium ions to doses of 1×10^{15} cm^{-2} (1) and 4×10^{15} cm^{-2} (2) at room temperature.

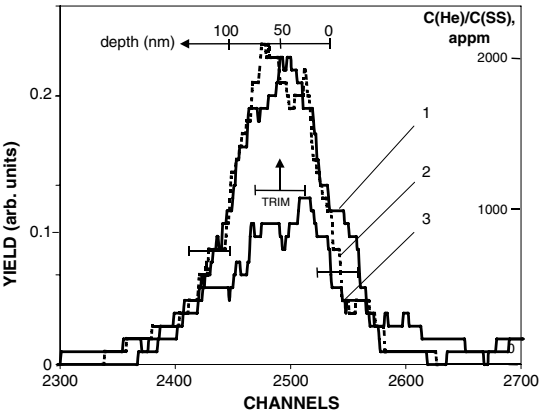

Fig. 2. Helium distribution profiles observed in 18Cr10NiTi steel irradiated with 10 keV helium ions to 1×10^{15} cm^{-2} at room temperature (1); annealed at temperatures 900 (2) and 1100 K (3).

decrease of ~30%. The decrease depends on the exposure time at a given temperature. Exposure of irradiated specimens at temperatures of 1100–1300 K for a few tens of seconds (a simulation of the thermal desorption experiment) does not cause variations in helium distribution profiles.

The temperature ranges of helium retention following implantation with energy 12 keV at room temperature to doses of 5×10^{14}–5×10^{16} cm^{-2} were determined by thermal-desorption mass spectrometry (Fig. 3). In the thermal desorption spectra obtained for irradiation doses 5×10^{14}–5×10^{15} cm^{-2} only one clearly defined peak is observed with a maximum at temperature 1360 K and width ~200 K (see Fig. 3, curves 1, 2).

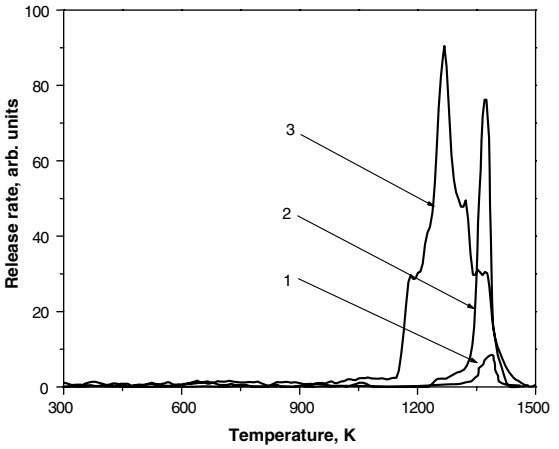

Fig. 3. Thermal desorption spectra of helium from 18Cr10NiT steel irradiated at 290 K by He^+ ions to doses of 5×10^{14} (1); 5×10^{15} (2); 5×10^{16} cm^{-2} (3).

At higher implantation doses helium desorption starts at lower temperatures. At a dose of 5×10^{16} cm^{-2} helium release begins at ~1100 K, passes through several stages and is completed at ~1500 K (see Fig. 3, curve 3). The maximum helium desorption is observed at ~1240 K in this case. At a dose of 5×10^{15} cm^{-2} the characteristic peak of thermal desorption at 1360 K becomes considerably lower. At an increased implantation temperature of ~900 K and high helium dose of $\sim5\times10^{16}$ cm^{-2} a decrease in peak height is observed in comparison with implantation at room temperature and the helium release appears as a single peak at ~1360 K.

Microscopy examination of helium-implanted specimens showed that helium bubbles following room temperature implantation were only observed for doses $>7\times10^{16}$ cm^{-2}. At lower helium doses annealing at elevated temperature was required to produce visible bubbles, with the size and distribution of bubbles dependent on the annealing temperature and time. Figs. 4–6 demonstrate the inability to see bubbles below 7×10^{16} cm^{-2} and the effect of annealing to produce visible bubbles.

3.2. Deuterium only

Deuterium distribution profiles were obtained in the dose range 2×10^{15}–4×10^{16} cm^{-2}. Fig. 7 shows deuterium distribution profiles in 18Cr10NiTi steel irradiated with 5 keV D^+ to 1×10^{16} cm^{-2} at room temperature. These profiles have rather smeared-out peaks with maximum depth distribution and peak width exceeding values calculated by the TRIM code. Even after taking into account profile broadening associated with depth resolution limits, the distribution width exceeds the calculated value by 30–50%.

Fig. 4. Microstructure of steel 18Cr10NiTi irradiated by helium ions with energy 12 keV at room temperature up to the dose 1×10^{16} cm^{-2}.

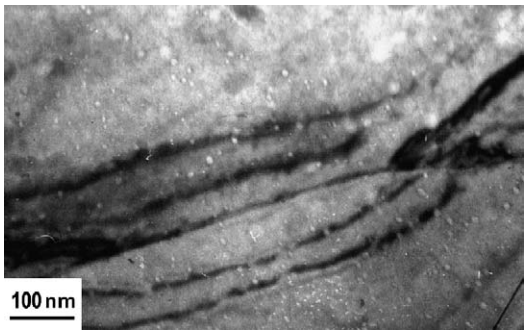

Fig. 5. Microstructure of steel 18Cr10NiTi irradiated by helium ions with energy 12 keV at room temperature up to the dose 2×10^{15} cm^{-2} and annealed at 1170 K for ~10 s.

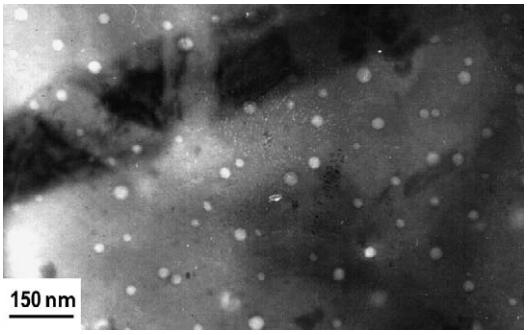

Fig. 6. Microstructure of steel 18Cr10NiTi irradiated by helium ions with energy 12 keV at room temperature to a dose 2×10^{15} cm^{-2} and annealed at 1170 K for 1800 s.

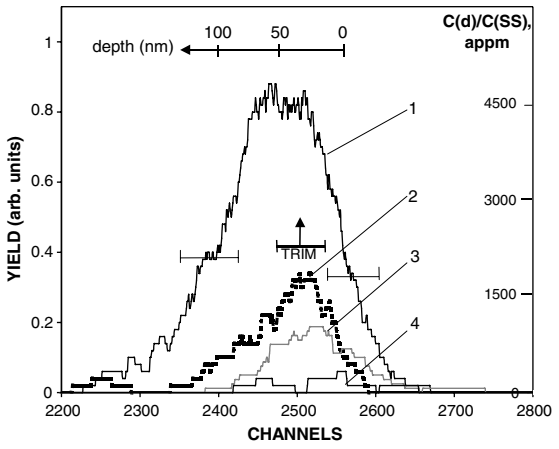

Fig. 7. Distribution profiles of deuterium implanted to 1×10^{16} cm^{-2} at room temperature (1) and after annealing at 380 (2); 500 (3) and 800 K (4).

The amount of deuterium retained in specimens at room temperature is 50–70% for spectra set up times of ~50–15 min, respectively, indicating some loss of deuterium during the profile measurement. The height and distribution width both decrease during annealing. In comparison with the amount retained at room temperature the amount of retained deuterium after annealing at 380, 500 and 800 K was 24%, 14% and 7%, respectively.

A typical thermal desorption spectrum for deuterium irradiation at 290 K to 10^{14}–10^{16} cm^{-2} has a relatively simple structure. One major peak with two weakly resolved maxima at temperatures 380 and 430 K is always observed (see Fig. 8).

With dose increasing from 1×10^{14}–1×10^{16} cm^{-2} the amplitude of the D^+/cm^2 peak increases and the temperature range of gas release shifts to higher temperatures. The amount of released deuterium for all implantation doses (corrected for a reflection factor of ~0.1 [18]) for 6 keV D^+ ions is ~90% of the implanted dose. Desorption is complete by 600 K. At 1×10^{16} D^+/cm^2 and higher a weak re-emission of D_2 is observed during irradiation. It appears that this emission causes a decrease of 20% of retained deuterium when increasing the nuclear reaction spectrum set up time from 15 to 50 min.

Microscopy examination of specimens implanted at room temperature only with deuterium and subsequently annealed at temperatures and times relevant to this experiment showed no cavities. Therefore no micrographs are presented for these specimens.

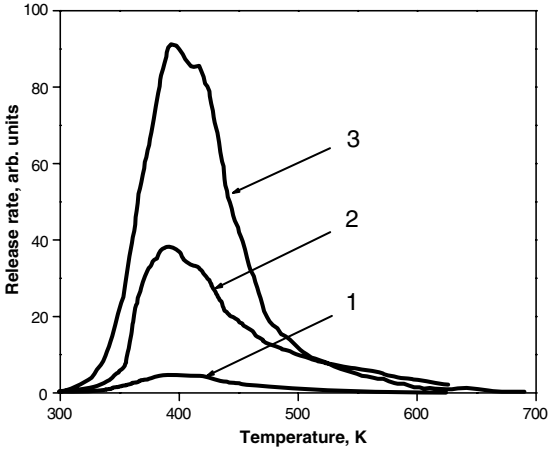

Fig. 8. Deuterium thermal desorption spectra from 18Cr10NiTi irradiated at 300 K to 1×10^{14} (1); 1×10^{15} (2) and 1×10^{16} D^+/cm^2 (3).

3.3. Helium + deuterium

The influence of helium pre-implantation on deuterium accumulation and retention in 18Cr10NiTi steel implanted at 5 keV was investigated for deuterium doses of 2×10^{15}–1×10^{16} cm^{-2}. Helium ions were implanted with energy 12 keV at room temperature to doses of 5×10^{15} and 5×10^{16} cm^{-2}. Deuterium was then implanted at room temperature.

Fig. 9 shows the post-annealing distribution profiles of deuterium implanted at room temperature to 1×10^{16} cm^{-2} into a specimen pre-implanted with helium to 5×10^{15} cm^{-2} following annealing at temperatures 290–800 K. In this case the implanted deuterium concentration reaches ~1.5 at.% for the 290 K case. Upon annealing at 380, 500 and 800 K the retained deuterium was 80%, 20%, and 10%, respectively, of the 290 K value.

When the helium dose is increased to 5×10^{16} cm^{-2} the concentration of retained deuterium again reaches ~1.5 at.% and is not changed by annealing until the temperature exceeds 500 K. The distribution profiles also remain unchanged for annealing below 500 K, confirming this conclusion (Fig. 10). Such a situation is also observed for deuterium implantation doses in the range 2×10^{15}–1×10^{16} cm^{-2}. Figs. 9 and 10, when compared to Fig. 7, clearly show that the presence of helium significantly increases the trapping of deuterium.

By processing of depth distribution profiles presented in Figs. 7, 9 and 10 the values of deuterium retention (R) were obtained. The temperature

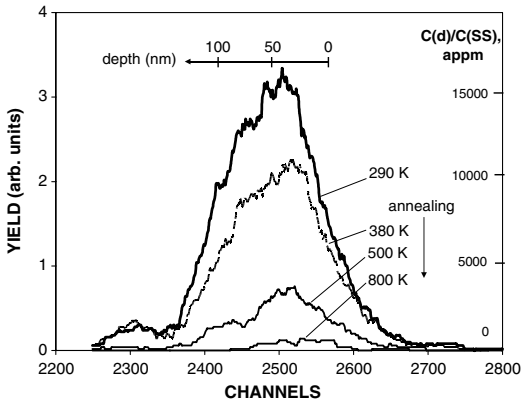

Fig. 9. Post-annealing distribution profiles of deuterium implanted to 1×10^{16} cm^{-2} after pre-implantation of helium to 5×10^{15} cm^{-2}, both injected at room temperature. Annealing temperatures are shown.

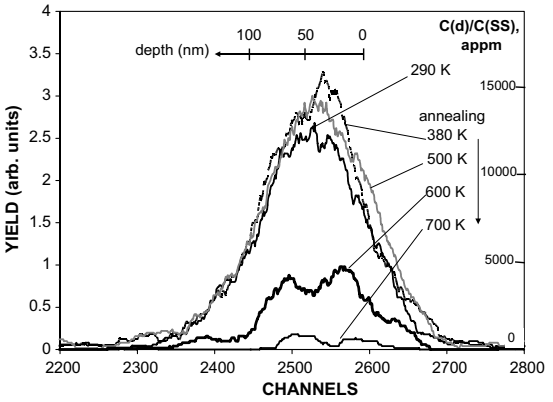

Fig. 10. Depth distribution profiles of deuterium implanted to 1×10^{16} cm^{-2} at room temperature and after annealing (pre-implanted helium at 5×10^{16} cm^{-2}).

dependencies of deuterium retention R are shown in Fig. 11. In specimens with pre-implanted helium the retained deuterium prior to annealing is ~90–100 % of the implanted value, but for implantation of deuterium alone this value equals only ~60%.

Thermal desorption spectra obtained in the case of implantation of helium and hydrogen are shown in Figs. 12 and 13. The simultaneous determination by thermal-desorption mass-spectrometry of desorbed deuterium and helium is difficult due to their equal mass. In this case H_2 and He are usually used. It is known that the mass difference of deuterium and hydrogen can influence the determination of the thermal-dynamic parameters (via the well-known isotope effect). However, no differences were observed in thermal desorption spectra upon change of deuterium to hydrogen [19].

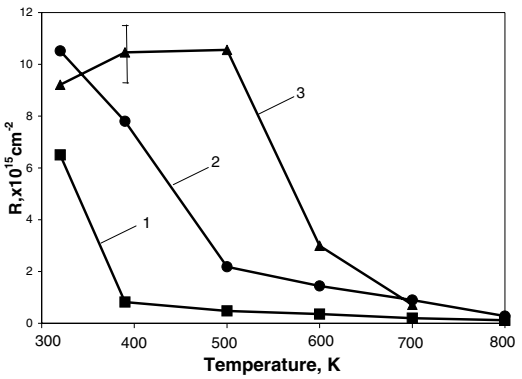

Fig. 11. Deuterium retention in 18Cr10NiTi steel implanted to 1×10^{16} cm^{-2} without helium (1) and with helium to 5×10^{15} (2) and to 5×10^{16} cm^{-2} (3).

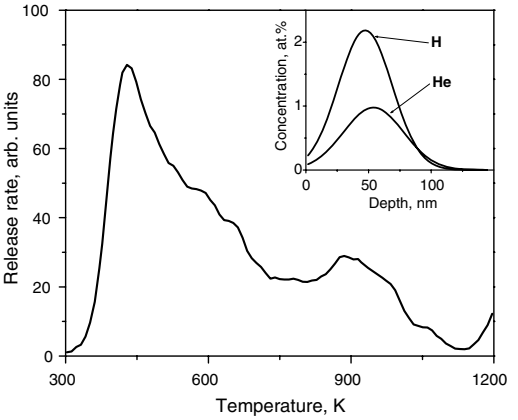

Fig. 12. Thermal desorption spectrum of hydrogen from specimen with H_2^+ ions at 300 K to 1×10^{16} H$^+$/cm^2 after helium pre-implantation to 5×10^{15} He$^+$/cm^2.

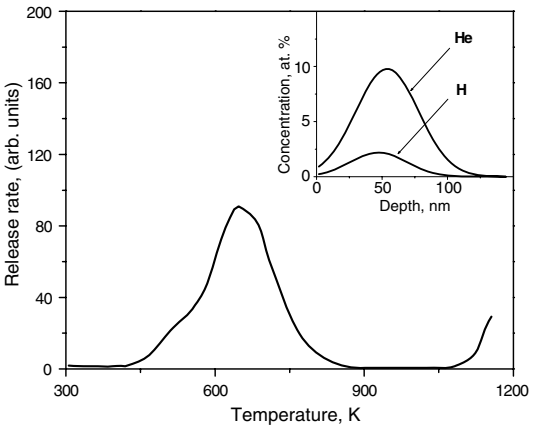

Fig. 13. Thermal desorption spectrum of hydrogen from specimen with H_2^+ ions at 300 K to 1×10^{16} H$^+$/cm^2 after helium pre-implantation to 5×10^{16} He$^+$/cm^2.

The thermal desorption spectrum from a specimen where hydrogen was implanted at 290 K to 1×10^{16} cm^{-2} (pre-implanted helium at 5×10^{15} cm^{-2}) exhibits hydrogen release over a wide temperature range with two well-defined maxima at ~420 K and ~900 K (Fig. 12).

Fig. 13 shows the desorption spectrum of hydrogen implanted to 1×10^{16} H$^+$/cm^2 after helium pre-implantation to 5×10^{16} cm^{-2}. It is seen at this higher helium level, that up to temperatures of ~500 K, gas release is negligible and only above this temperature does hydrogen release start, with a maximum release rate at 650 K. As noted earlier, specimens implanted with H_2^+ were heated only to 1200 K to avoid hydrogen release from chamber components. The relationship of helium and hydro-

gen profiles for Figs. 12 and 13 are presented in the inserts on the figures. The inserted profiles were calculated with the TRIM code.

Investigation of the microstructural evolution of helium implanted steel after irradiation at different temperatures and following post-implantation annealing has shown that at room temperature only dislocation structure was developed. At 5×10^{15} cm^{-2} only 'black spots' formed, but at 5×10^{16} cm^{-2} a more complicated dislocation structure was developed (see Figs. 14 and 15). Dislocation structure was also developed in specimens with different content of hydrogen. Increasing the annealing temperature caused a decreasing density of dislocation structure.

Following irradiation with hydrogen and helium ions and after subsequent annealing at 600 K a dislocation network was observed to develop at a helium dose of 5×10^{15} cm^{-2}. While bubbles may exist at small sizes at this dose, bubble formation was observed at a helium dose of 5×10^{16} cm^{-2} (see Figs. 16 and 17).

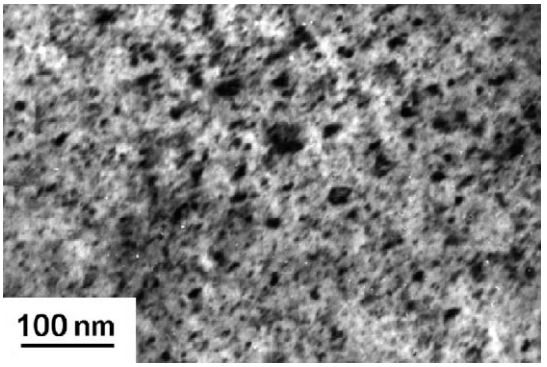

Fig. 14. Microstructure of 18Cr10NiTi steel irradiated with 12 keV helium ions at room temperature to 5×10^{15} cm^{-2}.

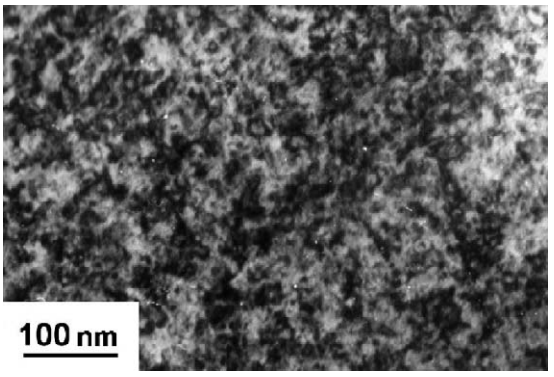

Fig. 15. Microstructure of 18Cr10NiTi steel irradiated with helium ions at room temperature to 5×10^{16} cm^{-2}.

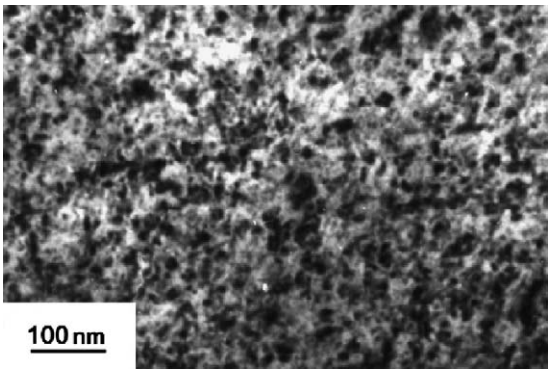

Fig. 16. Microstructure of 18Cr10NiTi steel irradiated with helium ions at room temperature to 5×10^{15} cm^{-2} and with hydrogen to 1×10^{16} cm^{-2} and then annealed at 600 K.

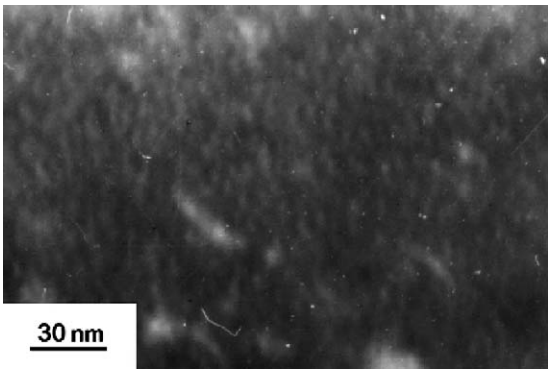

Fig. 17. Microstructure of 18Cr10NiTi steel irradiated with helium ions at room temperature to 5×10^{16} cm^{-2} and then with hydrogen to 1×10^{16} cm^{-2} and subsequently annealed at 600 K. Very small, difficult to see, bubbles are located throughout the matrix.

3.4. Chromium + deuterium

In the case where 18Cr10NiTi stainless steel specimens were first irradiated by Cr^{3+} ions to 50 dpa, the retained deuterium concentration is found to increase. Fig. 18 shows the distribution profiles of deuterium implanted at room temperature to a dose of 1×10^{16} cm^{-2} in the initial state compared with the profile of a specimen irradiated by Cr^{3+} ions. Comparison of the profiles shows that after irradiation at 290 K and after annealing, the concentration of deuterium is higher and the half width of the distribution is larger when the specimens have been previously irradiated with Cr ions.

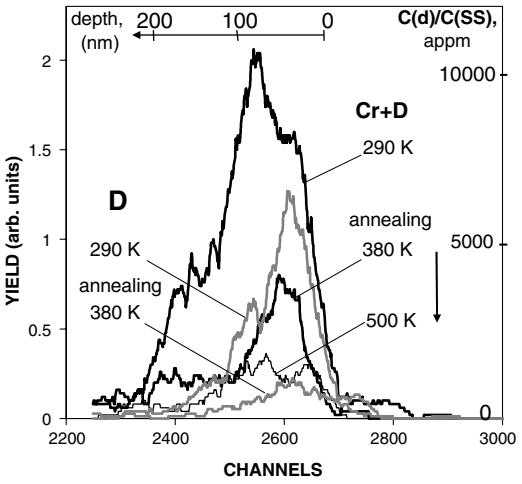

Fig. 18. The distribution profiles of deuterium implanted to 1×10^{16} cm^{-2} at room temperature and after annealing at 380 and 500 K, compared to the specimen with similar implantation that had been previously irradiated with Cr^{3+}.

The amount of deuterium retained in the Cr-implanted specimen after annealing at temperatures of 380, 500 and 800 K is 40%, 20% and 2% with respect to the amount of deuterium retained at room temperature.

As one can see in Fig. 19 TRIM calculation for high exposure indicates that the level of displacement damage increases almost linearly with depth from the surface. It increases about a factor of two from 0 to 0.4 μm, peaking at 120 dpa but averaging ~50–60 dpa in the gas-implanted and examined region of 0–0.15 μm.

Deuterium has significant mobility at room temperature. During its migration through the chromium damaged layer it is becoming fixed in traps created by Cr^{3+} ions. As a result the deuterium distribution profiles are observed to widen. A decrease in the concentration level always takes place during annealing, but the capture and retention of deuterium following Cr^{3+} ion irradiation is several times higher compared to the capture by defects created by irradiation by deuterium alone.

In the case of preliminary irradiation by Cr^{3+} ions we observe a shift of the temperature intervals of deuterium release towards the high temperature region and a redistribution of the intensities in each of the peaks (Fig. 20). Unlike the case with the original 18Cr10NiTi steel specimens where after deuterium irradiation the main thermo-activated release was observed at 390 K (70%), in the case of preliminary Cr^{3+} ion irradiation, deuterium is released at 500–750 K (75%). The relative intensity relationship for the peaks at 390, 480 and 700 K is 25%, 55% and 20%, respectively.

The situation of most interest is when displacive irradiation proceeds at reactor-relevant temperatures. Fig. 21 shows the structure that developed over the depth of 0–150 nm in 18Cr10NiTi steel after irradiation to 50 dpa by Cr^{3+} ions at 920 K. Formation of a dislocation network and faceted voids (~4.3 nm mean size with density of 1.5×10^{15} cm^{-2}) was observed.

Based on results by Garner et al. it appears that voids may be even more effective than bubbles at storing hydrogen [4,5]. Based on the data presented above, one may assume that formation of a dislocation network with high density of voids will also result in strong accumulation and retention of hydrogen–deuterium isotopes in 18Cr10NiTi steel

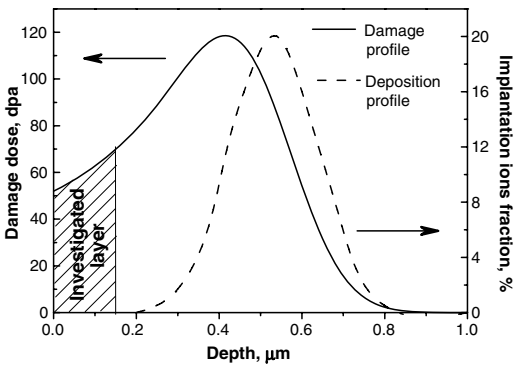

Fig. 19. Typical calculated distribution profile of chromium ions injected with energy of 2 MeV and the resultant damage profile.

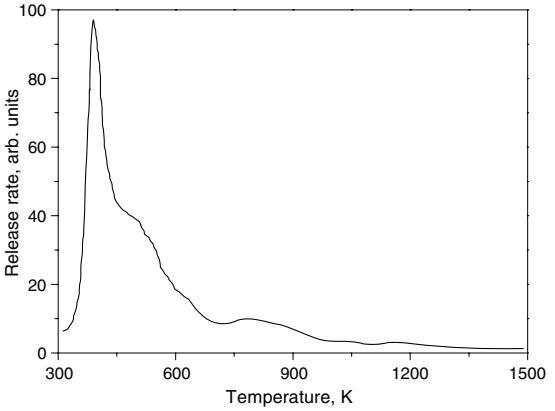

Fig. 20. Thermo-desorption in 18Cr10NiTi steel of deuterium implanted to 1×10^{17} cm^{-2} at room temperature after preliminary irradiation with Cr^{3+} ions to 50 dpa.

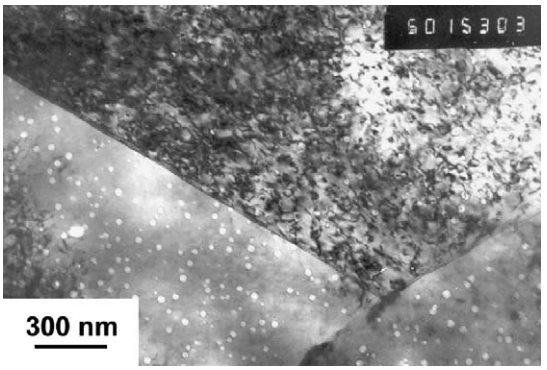

Fig. 21. Microstructure of 18Cr10NiTi steel over the depth of 0–150 nm after irradiation by Cr^{3+} ions at 920 K up to 50 dpa at this depth.

up to temperatures of 800–1000 K. This possibility is now the subject of on-going investigations.

It should be noted that the data derived using chromium ions were obtained via irradiation in two accelerators in separate test chambers, whereas the hydrogen and helium irradiations were performed in only one chamber and accelerator. Specimens were transferred from one chamber to the other, thus allowing contact with air over 1–2 days between the two irradiations. Contact of the specimens with the air between the irradiations may result in some surface change of the 18Cr10NiTi steel. Additional tests are being conducted now to define the effect of the specimen's contact with the air on deuterium retention in the 18Cr10NiTi steel.

4. Discussion

In the 1980s the issue of synergetic effects of simultaneous implantation of helium and hydrogen on defect structure evolution and on mechanical properties of the fusion reactor first wall was considered in a number of studies. The data obtained in those studies showed a rather complicated influence of simultaneous implantation of these gases on microstructure development.

The results of more recent studies had demonstrated that simultaneous irradiation with self-ions; helium and hydrogen can lead to a significant acceleration of void swelling relative to that generated in environments where the hydrogen level is low. For example, simultaneous irradiation of self-ions, He^+ and H^+ ions was observed to increase swelling strongly in ferritic steel [20] and in vanadium [21]. Hardening in austenitic steel 316 SS [22] is two times higher in comparison with dual irradiation (Fe^{3+}, He^+ or Fe^{3+}, H^+) or separately by helium and hydrogen, indicating a strong role of trapping. In a number of cases, however, a suppression of swelling is observed after implantation of helium and hydrogen [9]. The complicated effect of simultaneous implantation of helium and hydrogen on microstructural development is obviously rather sensitive to the peculiarity of each material and environment.

In Ref. [23] deuterium trapping in nickel, iron, copper, stainless steel, and aluminum was studied. All of these materials were irradiated at 100 K. It was shown that pre-implantation of helium produced additional traps for deuterium and shifted the temperature range of its release from nickel, iron, copper, and stainless steel from 240–300 to 350–500 K. The authors of that study assumed that helium bubbles were the operating traps and deuterium must be chemisorbed on the bubble walls. Data presented for aluminum appear to confirm this conclusion, since it was shown that helium pre-implantation did not shift the deuterium release temperature, probably due to aluminum's low heat of deuterium chemisorption. On the other hand, the elastic fields around defect clusters such as bubbles are considered by some researchers as the trap for retaining hydrogen [24].

Results obtained in the current paper for stainless steel 18Cr10NiTi show that pre-implantation of helium causes the accumulation and retention of practically all deuterium implanted to concentrations of 3000–15 000 appm. For room temperature irradiation the efficiency of deuterium trapping is found to be the same for helium doses that differ by one order of magnitude. Deuterium retention at elevated temperature differs for helium pre-implantation to 5×10^{15} and 5×10^{16} cm^{-2}. This conclusion is confirmed by thermo-desorption data (see Figs. 12 and 13), profile evolution (Figs. 9 and 10) and temperature dependence of deuterium retention (Fig. 11).

For helium at 5×10^{15} cm^{-2} the decrease of concentration (Fig. 9) and release of deuterium from specimen (Fig. 12) takes place after annealing at temperature 360 K. But on comparison with D_2^+ irradiation only, (Fig. 11, curve 1) deuterium retention in the case of helium pre-implantation is several times higher and the temperature range of release is considerably wider.

For helium at 5×10^{16} cm^{-2} deuterium is retained in 18Cr10NiTi to annealing temperatures of ~500 K; this is illustrated by the invariability of

deuterium distribution profiles (Fig. 10) and the absence of deuterium release (Fig. 13). Such behavior is obviously caused by deuterium capture at stronger traps produced by helium implantation. The formation of new types of traps with increasing helium implantation ($5\times10^{15}\,cm^{-2}$ to $5\times10^{16}\,cm^{-2}$) is demonstrated by changes in the gas release spectra. The structure became more complicated, additional new peaks appear, and changes occur in their relative intensity (Fig. 3).

Microscopy investigation has demonstrated significant differences in microstructure with changing levels of pre-implanted helium. For smaller doses only dislocation structure was observed. A ten-fold increase of helium caused increasing amounts of helium bubbles to form in the microstructure.

Our results on trapping and retention of deuterium on dislocation structure and bubbles indicate that the most effective deuterium retention occurs in the case of bubble structure development. In the latter case the temperature range of deuterium trapping broadens up to ~1000 K and exceeds the temperature ranges of retention obtained for other materials [20–24]. It was also seen that high levels of damage induced by self-ions at room temperature were especially effective to trap hydrogen isotopes.

It is yet to be confidently verified that voids developed at much higher, reactor-relevant temperatures are even more efficient than bubbles at storing hydrogen, and whether there are any consequences of such storage on acceleration of void swelling or developing of IASCC, but additional experiments are now in progress to resolve some of these questions.

5. Conclusions

1. Results obtained in this paper for 18Cr10NiTi stainless steel show that ion implanted deuterium is weakly trapped by defects produced in 5 keV D^+ displacement cascades. The effective trapping temperature interval is 300–600 K.
2. Helium implantation into this steel causes the formation of traps that can retain hydrogen isotopes in a wider range of temperatures, 500–1000 K.
3. The characteristics of trapping and the temperature range of retention of hydrogen isotopes in traps formed by prior implantation of helium depends on the concentration of implanted helium and on the type of developed defects.
4. Formation of helium bubbles in 18Cr10NiTi steel causes an increase of retained deuterium by one order of magnitude in the range 350–550 K.
5. When the damage level is strongly increased by prior irradiation with Cr^{3+} ions the level of retention is also strongly increased.
6. These results support the possibility that displacive irradiation of stainless steels in nuclear environments that produce large amounts of helium and hydrogen will experience enhanced trapping of significant amounts of hydrogen, with possible consequences on the onset and amount of void swelling, development of hardening and possibly on corrosion and cracking.

Acknowledgements

The majority of this work was conducted with support from the Science and Technology Center in Ukraine under STCU grant support, Project N 2149. The relatively small US portion of this effort was jointly sponsored by the Materials Science Branch, Office of Basic Energy Sciences, and the Office of Fusion Energy, US Department of Energy.

The strong assistance of Natalia Brikotnina of Interpreter and Translation Services to assist in the development and translation of this work is very much appreciated.

References

[1] F.A. Garner, B.M. Oliver, L.R. Greenwood, M.R. James, P.D. Ferguson, S.A. Maloy, W.F. Sommer, J. Nucl. Mater. 296 (2001) 66.
[2] B.M. Oliver. F.A. Garner, S.A. Maloy, W.F. Sommer, P.D. Ferguson, M.R. James, in: S.T. Rosinski, M.L. Grossbeck, T.R. Allen, A.S. Kumar (Eds.), Proceedings of Symposium on Effects of Radiation on Materials, 20th International Symposium, ASTM STP 1405, American Society for Testing and Materials, West Conshohocken, PA, 2001, p. 612.
[3] T.P. Peng, C.J. Alstetter, Acta Metall. 34 (1986) 1771.
[4] F.A. Garner, B.M. Oliver, L.R. Greenwood, D.J. Edwards, S.M. Bruemmer, Ninth International Symposium on Environmental Degradation of Materials in Nuclear Power Systems – Water Reactors, Tahoe (2001) 54.
[5] F.A. Garner, E.P. Simonen, B.M. Oliver, L.R. Greenwood, M.L. Grossbeck, W.G. Wolfer, P.M. Scott, these Proceedings, doi:10.1016/j.jnucmat.2006.05.023.
[6] F.A. Garner, L.R. Greenwood, D.L. Harrod, Sixth International Symposium on Environmental degradation of Materials in Nuclear Power Systems – Water Reactors (1993) 783.
[7] F.A. Garner, D.J. Edwards, S.M. Bruemmer, S.I. Porollo, Yu. V. Konobeev, V.S. Neustroev, V.K. Shamardin, A.V. Kozlov, in: Proceedings, Fontevraud 5, Contribution of

Materials Investigation to the Resolution of Problems Encountered in Pressurized Water Reactors, 23–27 September, 2002, paper #22, on CD format.
[8] I.M. Neklyudov, G.D. Tolstolutskaya, Helium and Hydrogen in Structural Materials, in: Questions of Atomic Science and Techniques (VANT) in Series: Physics of Radiation Damage and Radiation Material Science, vol. 83, N3, 2003, p. 3 (in Russian).
[9] I. Mukouda, Y. Shimomura, T. Iiyama, J. Nucl. Mater. 283–287 (2000) 302.
[10] I.M. Neklyudov, L.S. Ozhigov, B.A. Shilyaev, I.N. Laptev, A.A. Parkhomenko, A.N. Morozov, V.V. Bryk, O.V. Borodin, Hydrogen in Stainless Steels of Pressure Vessel Internals of Reactor WWER-1000, in: Questions of Atomic Science and Techniques (VANT) in Series: Physics of Radiation Damage and Radiation Material Science, vol. 83, 2003, p. 58 (in Russian).
[11] L.R. Greenwood, F.A. Garner, J. Nucl. Mater. 233–237 (1996) 1530.
[12] F.A. Garner, B.M. Oliver, L.R. Greenwood, J. Nucl. Mater. 258–263 (1998) 1740.
[13] F.A. Garner, L.R. Greenwood, B.M. Oliver, ASTM STP 1325, in: R.K. Nanstad, M.L. Hamilton, F.A. Garner, A.S. Kumar (Eds.), Effects of Radiation on Materials: 18th International Symposium, American Society of Testing and Materials, 1999, p. 794.
[14] G.D. Tolstolutskaya, I.M. Neklyudov, F. Zelenskiy, V.V. Bryk, I.E. Kopanetz, V.V. Ruzhitskyi, V.I. Bendikov, S.A. Karpov, Diagnostics by in situ Method of Nuclear Reactions of Hydrogen and Helium Implanted into 08Cr18Ni10Ti Steel, in: Proceeding of XV International Conference on Physics of Radiation Phenomena and Radiation Materials Science, Alushta, Ukraine, 10–15 June 2002, p. 225 (in Russian).
[15] B.M.U. Scherzer, H.L. Bay, R. Behrisch, B. Borgesen, J. Roth, Nucl. Instrum. and Meth. 157 (1978) 75.
[16] A. Karpov, I.E. Kopanetz, I.M. Neklyudov, V.V. Ruzhytskiy, G.D. Tolstolutskaya, Combination of nuclear reactions method, thermodesorption spectrometry and two-beam irradiation at investigation of helium and deuterium behaviour in constructive materials, in: Proceeding of XIV International Conference on Radiation Physics of Solids, Sevastopol, Ukraine, 05–10 July 2004, p. 592 (in Russian).
[17] J.F. Ziegler, J.P. Biersack, U. Littmark, The Stopping and Ranges of Ions in Solids, Pergamon, New York, 1985.
[18] S. Yamaguchi, S. Nagata, K. Takahito, S. Yamamoto, J. Nucl. Mater. 220–222 (1995) 878.
[19] V.F. Rybalko, V.V. Ruzhytskiy, G.D. Tolstolutskaya, V.I. Bendikov, Simulation and Study of Thermonuclear Plasma Interaction with Structural Materials' Surface on Charged Particle Accelerators and on Plasma Assemblies, Report N Y67256, Kharkov, 1983, p. 195 (in Russian).
[20] T. Tanaka, K. Oka, S. Ohnuki, S. Yamashita, T. Suda, S. Watanabe, E. Wakai, J. Nucl. Mater. 329–333 (2004) 294.
[21] N. Sekimura, T. Iwai, Y. Arai, S. Yonamine, A. Naito, Y. Miwa, S. Hamada, J. Nucl. Mater. 283–287 (2000) 224.
[22] J.D. Hunn, E.H. Lee, T.S. Byun, L.K. Mansur, J. Nucl. Mater. 282 (2000) 131.
[23] S.M. Myers, P.M. Richards, W.R. Wampler, F. Besenbacher, J. Nucl. Mater. 165 (1989) 9.
[24] S. Nagata, K. Takahiro, J. Nucl. Mater. 290–293 (2001) 135.